PCCP

PERSPECTIVE

View Article Online
View Journal | View Issue

Cite this: *Phys. Chem. Chem. Phys.*, 2014, **16**, 23515

Recent advances in anisotropic magnetic colloids: realization, assembly and applications

Pietro Tierno[ab]

Received 15th July 2014,
Accepted 28th August 2014

DOI: 10.1039/c4cp03099k

www.rsc.org/pccp

This perspective article will give an overview of recent experimental results related to the realization and use of anisotropic magnetic colloids, *i.e.* microscopic particles having the shape, composition or structured surface which set a preferred magnetization direction. The possibility of remotely controlling these soft matter building blocks *via* external fields makes them ideal for a wide range of applications, from their use as active microrheological probes to infer the viscoelastic properties of complex fluids to their implementation as active systems in microfluidic devices. This article will also review the recent use of these anisotropic units as field driven or guided propellers, which can be magnetically moved or guided in a fluid medium, thus being potentially useful in precise single-particle drug delivery operations.

1 Introduction

Colloidal systems, here focusing on fluid suspensions of polymer microspheres, are interesting not only because of their ubiquitous technological nature, but also because of their mesoscopic character, with length and time scales unmatched by more "traditional" systems such as atomic, molecular or granular ones. When colloidal particles are made using (or coated with) magnetic materials, they become responsive to external fields, and the resulting magnetic interactions can be precisely tuned. An external magnetic field can be oriented in such a way to induce attractive or repulsive interactions between the particles, while its amplitude controls the interaction strength.

In contrast to isotropic particles, anisotropic magnetic colloids are characterized by an induced or spontaneous magnetization which has a dependence on a particular direction. Magnetic anisotropy can result from several factors, like from the magneto-crystalline structure of the material, the particle shape, the presence of stresses, surfaces or interfaces between different materials as already described in the literature.[1] These magnetic particles are characterized by anisotropic and directional interactions, and can give rise to highly complex structures and dynamics, bringing novel physical questions and challenges. As a matter of fact, particle shape and interactions affect the fundamental aspects of colloidal behaviour, from Brownian motion[2] to crystal formation,[3] frustration[4] and glassy behaviour.[5] On the application side, when compared to isotropic particles, anisotropic colloids feature the advantages of being easily torqued by an external field and the corresponding orientation being visualized by simple optical techniques. These properties can be employed in several applications, where anisotropic magnetic particles are used as force sensors, microstirrers, active components in constrained geometries, microrheological probes or externally actuated micropropellers.

This perspective article describes recent experimental progress in realizing and using anisotropic magnetic colloids. It will focus on systems with a micron length, where particle assembly and dynamics in the dispersing medium are readily accessible *via* simple optical techniques such as particle tracking.[6] It is organized into three sections. The first one will describe different strategies used to produce these particles. The second will first give a few theoretical ingredients related to the particle

[a] *Departament de Estructura i Constituents de la Matèria, Universitat de Barcelona, Av. Diagonal 647, 08028 Barcelona, Spain. E-mail: ptierno@ub.edu; Tel: +34 9340 34031*
[b] *Institut de Nanociència i Nanotecnologia IN²UB, Universitat de Barcelona, Barcelona, Spain*

Pietro Tierno

Pietro Tierno studied physics at the University "Federico II" of Napoli, and received a PhD in Natural Sciences from the University of Ulm in 2005. After a postdoc at Florida State University, he moved to the University of Barcelona in 2007, where now he is "Ramon y Cajal" researcher. In 2013 he received an ERC Starting Grant from the European Research Council. His research interests focus on soft condensed matter systems with emphasis on manipulation and transport of colloidal particles, propulsion in viscous fluids and self-assembly phenomena.

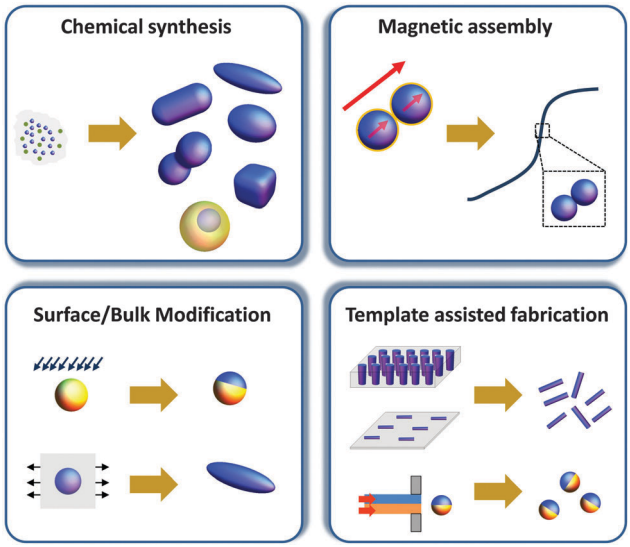

Fig. 1 Schematic showing different strategies to produce anisotropic magnetic colloids.

dynamics and interactions under an external field. Then it will describe different types of assembled structures. The last and more extended section will focus on the applications.

2 Preparation methods

Fig. 1 illustrates four different and sometimes complementary approaches to realize anisotropic magnetic colloids. Direct chemical synthesis allows obtaining a wide variety of shapes or sizes or even to produce, *via* multistep processes, complex composite particles characterized by a magnetic core or shell. Elongated structures such as chains or filaments can be assembled *via* attractive dipolar interactions and later permanently linked by using a proper chemical functionalization. A different approach consists of the modification of the particle surface or bulk *via* metal deposition or mechanical elongation, respectively. Finally, anisotropic particles can be engineered following various template assisted growth processes, including electrodeposition in a porous membrane, microtransfer moulding or photopolymerization in a microfluidic channel.

2.1 Chemical synthesis

There are several methods to synthesize microscopic metallic particles, and a detailed account of all these techniques is a formidable task which has been given in several excellent reviews.[7–11] Here will be described few of these methods which have been recently formulated or reproposed.

Perhaps one of the simplest ways to obtain monodisperse anisotropic magnetic particles involves letting age condensed ferric hydroxide solutions, as pioneered by Matijević and co-workers several years ago.[16] Along the same lines, Sugimoto *et al.* developed a "gel-sol" method to produce anisotropic hematite (α-Fe_2O_3) particles with a variety of shapes, like pseudocubes, ellipsoids and peanuts.[17,18] The process consisted of mixing $FeCl_3$ and NaOH with various amount of Na_2SO_4 and leaving the resulting solution at ~100 °C for ~8 days. Fig. 2(a–d) show different shapes obtained by adjusting the concentration of sulfate ions. Due to the simplicity and high yield, this technique has been recently reproposed by various groups to study the particle aggregation under external fields,[13] or to use these particles as a template for the controlled growth of monodisperse silica shells.[19,20] An interesting feature of the anisotropic hematite particles is the presence of a permanent dipole moment perpendicular to the particle crystalline axis (*c*-axis). This peculiarity can be explained by considering the magnetic structure of hematite.[21,22] As illustrated in Fig. 2(e),[13] hematite crystallizes in the corundum structures, in which the Fe cations are aligned antiferromagnetically along the *c*-axis. Above the Morin temperature, $T_M \sim 263$ K, the hematite becomes weakly ferromagnetic, with the magnetic spins lying mostly in the basal plane, and perpendicular to the *c*-axis.

Composite particles with fixed or mobile magnetic cores can be obtained *via* multi-step processes, where first the metallic core is synthesized, and later used as a seed to grow a larger nonmagnetic structure. The asymmetric doublets in Fig. 2(g) were produced by using Fe_3O_4 colloidal cores coated with a concentric shell of crosslinked polystyrene (PSt).[14] Swelling of the polymer network and subsequent phase separation were used to grow a bulb on one side of the particles. Fig. 2(h and i) show dried assembled structures formed by these composite particles under a static field. Particles with concentric cores generated linear chains (*h*), while zigzags chains were formed by eccentric particles in order to minimize the distance between the attractive magnetic cores. Using a three-step polymerization process, Nishi *et al.*[23] were able to synthesize anisotropic particles with a magnetic core and two protruding lobes. As demonstrated by Nagao *et al.*,[24] it was possible to mobilize the magnetic core by first coating the particles with a silica shell, and later removing the polymer material. The "yolk/shell" particle in Fig. 2(j) was realized by Okada *et al.*,[15] and was composed of a magnetic mobile core inside a hollow silica shell. During preparation, the core was covered by a PSt layer, which was subsequently coated by an additional silica shell, and heat treatment was used to dissolve the PSt.

Particles with mobile cores have attractive features, since they can be used to assemble superlattices with controllable magnetic inclusions. These colloidal crystals have potential applications in photonic band gap materials or filtration of magnetic fluids. As an example, Fig. 2(k) shows an ensemble of close-packed yolk/shell particles, with the magnetic cores visible as bright spots under an optical microscope. Application of an in-plane static field $H \sim 80$ kA m^{-1} forces the magnetic cores to approach each other and reconfigure the lattice of metallic inclusions without deforming the triangular packing of the shell particles.

2.2 Magnetic assembly

Attractive dipolar interactions are able to assemble isotropic particles into elongated chains, which can be used as magnetic stirrers[25,26] or to realize biomimetic structures such as artificial cilia,[27,28] besides their interesting physical properties.[29–31]

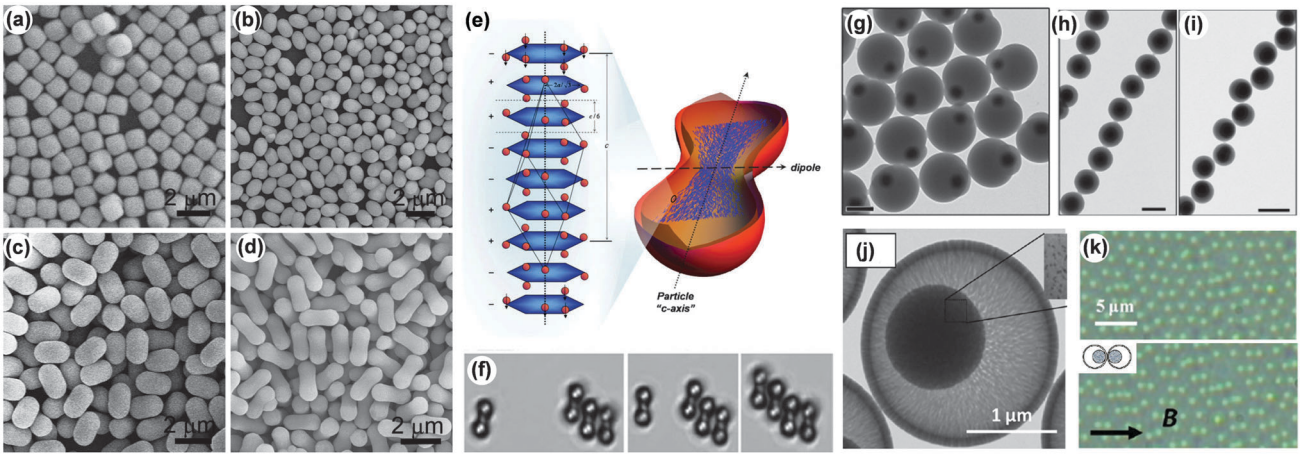

Fig. 2 (a–d) Scanning electron microscope (SEM) images of hematite pseudocubes (a), ellipsoids (b), capsules (c) and peanuts (d) obtained by aging condensed ferric hydroxide gels. (e) Schematic showing the magnetic ordering of a hematite particle. (f) Aggregation of magnetic peanuts. (g–j) Transmission electron microscope (TEM) images of Fe_3O_4/SiO_2/PS doublets (g), assembly of concentric (h) and eccentric (i) Fe_3O_4/SiO_2/PS particles under an external magnetic field. (j) TEM image of a yolk/shell particle and (k) particle assembly in the absence (top) and in the presence (bottom) of an external field. [(a–d) Reprinted with permission from ref. 12 (Copyright 2013 ACS), (e, f) from ref. 13 (Copyright 2012 Wiley), (g–i) from ref. 14 and (j, k) from ref. 15 (Copyright 2007 and 2013 ACS)].

To link the particles forming these chains, the simplest way would consist of screening the repulsive electrostatic interaction between the particles, in favor of attractive Van der Waals. This approach has been used in the past by adding to the dispersing medium (water) an electrolyte (NaCl)[32] or a polyelectrolyte (polyacrylic acid).[33] However, the stability of the chains obtained with this method was difficult to control, since adhesion *via* Van der Waals forces is thermally activated,[34] and thus chain fragmentation can easily occur with time.

More stable structures can be obtained *via* functionalization of the particle surface. The asymmetric doublets shown in Fig. 3(a) were produced by linking streptavidin coated paramagnetic microspheres with complementary DNA strands. A short length of 25 base pairs was chosen in order to produce stiff doublets. The DNA linkage was promoted by exposing a binary mixture of particles having 1 μm and 2.8 μm size to a constant field of $H = 4 \times 10^5$ A m^{-1} for ~15 min.[35] Increasing the exposure time could produce longer chains, while changing the length of the DNA bridge could modify the chain flexibility.[41]

Besides DNA, other chemical linkers can be used. Flexible magnetic filaments were realized by Furst *et al.*[32] with glutaraldehyde. Goubault *et al.*[36] realized filaments by linking ~600 nm magnetic colloids with absorbed polyacrylic acid (PAA). As shown in Fig. 3(c), depending on the chain length, different reorientation behaviour were found under the action of a static field. Short chains rotated as rigid rods (r), while longer chains bent into hairpins (h) or even deformed assuming a sinusoidal shape (s) for very long ones. By measuring the hairpin curvature *via* optical microscopy and the PAA length from diffracted light, the authors were able to extract the bending rigidity of the molecular linker. Biswal and Gast[37] realized magnetic filaments using particles covalently bound to streptavidin, and linked with a bisbiotin-poly(ethylene glycol) (PEG) molecule, Fig. 3(d). By adjusting the length of the PEG spacer, it was possible to change the chain

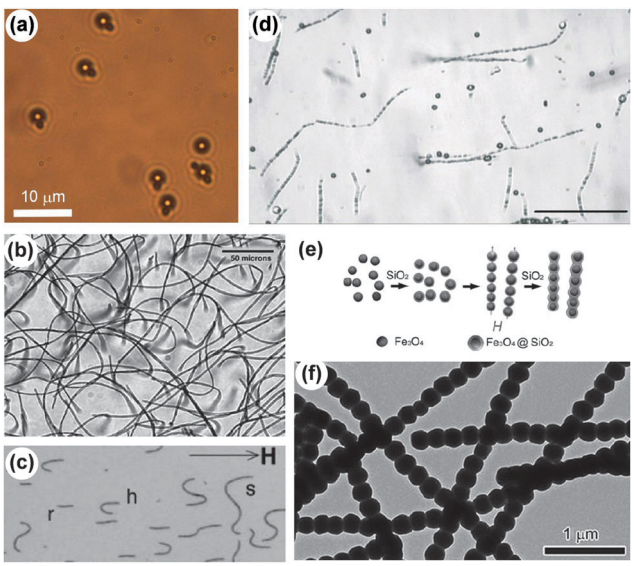

Fig. 3 (a) Anisotropic doublets linked *via* complementary DNA strands.[35] (b) Flexible magnetic filaments permanently linked by absorbed polyacrylic-acid and (c) deformation under a static field of amplitude H = 1.0 kA m^{-1}. (d) Magnetic filaments linked with polyethylene-glycol. (e, f) Stiff magnetic chains uniformly coated by a silica shell. [(b, c) Reprinted with permission from ref. 36 (Copyright 2003 APS); (d) from ref. 37 (Copyright 2003 APS); (e, f) from ref. 38 (Copyright 2011 Wiley)].

flexibility, and the bending stiffness, as measured *via* optical tweezers.

An alternative approach to produce stiff magnetic filaments was recently proposed by Hu *et al.*[38] using silica coating during the chaining process, Fig. 3(e). The method consisted of mixing aqueous dispersion of Fe_3O_4 particles with ammonium hydroxide and ethanol. A thin silica layer around the particles was grown by hydrolyzation and condensation of tetraethoxysilane injected in

the solution. Application of a low intense magnetic field ($H \sim 80$ A m^{-1}) at the initial stage of the process induced particle chaining, producing the stiff peapod-like structures showed in Fig. 3(f). It was possible to tune the chain length from few to tens of micrometers by varying the exposure time of the applied field during the chaining process.

2.3 Surface/bulk modification

Isotropic particles can become magnetic when the whole surface or a part of it is coated with a magnetic material such as Fe, Co or Ni. A thin metallic layer can be directly grown above the particle surface *via* a chemical process, like electroless plating,[42] can be formed *via* adsorption of small magnetic particles,[43] or upon metal evaporation.[44] The first two methods allow covering the whole particle surface, producing magnetic core–shell particles in the first case, or "colloidosomes" in the second one. Using the third method, the magnetic material can be deposited above one particle hemisphere, producing bi-functional "Janus" particles, with different physical and chemical properties at the two sides.[49,50]

Magnetic Janus particles have been realized by various groups *via* metal evaporation.[51,52] The procedure usually consists of forming a two dimensional monolayer of particles above a flat substrate or at a liquid interface, on top of which the metallic material is deposited.[49] The left part of Fig. 4(a) shows "half" magnetic Janus colloids realized from 10 μm PSt spheres. These particles were first convectively assembled above a glass substrate and later one hemisphere was covered by a 50 nm Co layer.[39] As shown in the right part of Fig. 4(a), it was possible to realize "dot" Janus colloids, with only 20% of the surface covered, by embedding the colloidal monolayer into a protecting photoresist. In contrast to half Janus particles, dot Janus were addressable by optical tweezers due to the small metallic coverage. Alternative approaches to produce magnetic Janus colloids have been reported by polymerizing magnetic nanoparticles in oil-in-water emulsion[53] or *via* sonochemical synthesis.[54]

A different method shown in Fig. 4(b) consists of the controlled mechanical deformation of isotropic magnetic colloids, to realize paramagnetic microellipsoids with a well defined aspect ratio. The original approach to elongate isotropic particles, as developed by Ho *et al.*,[55] consisted of dispersing the pristine particles in a thin film made by a thermoplastic material such as polyvinyl alcohol (PVA). The PVA film and the colloidal inclusions were stretched while immersed into an oil bath heated above the glass transition temperature of the particles. However this approach was unable to deform magnetic colloids due to the high viscosity of these particles, resulting from the presence of metallic inclusions.[56] The paramagnetic microellipsoids shown in Fig. 4(b) were obtained by using a variant of this technique, which employed a non-polar solvent (toluene) to liquefy the particles rather than heat treatment.[57] The procedure illustrated in the top part of Fig. 4(b) consisted of dispersing the pristine particles (1) in a PVA solution which was cast into a thin film, (1) → (2). Stripes of the film were clamped into a metal frame (2) → (3), and the frame immersed in a toluene bath, (3) → (4). After mechanical elongation (4) → (5), the magnetic ellipsoids were resolidified by extracting the frame from the toluene bath.

While these approaches are able to produce monodisperse particles with tailored magnetic coating (Janus colloids) or sharp ends (microellipsoids), compared to chemical synthesis their yield is limited by the fabrication process, or by the use of repeated washing and redispersing procedures to recollect the particles.

2.4 Template-assisted fabrication

Magnetic nanowires with a length of several micrometers can be grown on a porous membrane *via* electrodeposition. As shown in Fig. 5(a), the general process consisted of first depositing a thin metal film on a face of a sacrificial aluminium oxide membrane, in order to use the latter as a working electrode.[45] The membrane pores are then covered by a small amount of metal to avoid deformation at one end of the growing nanowires. The size of

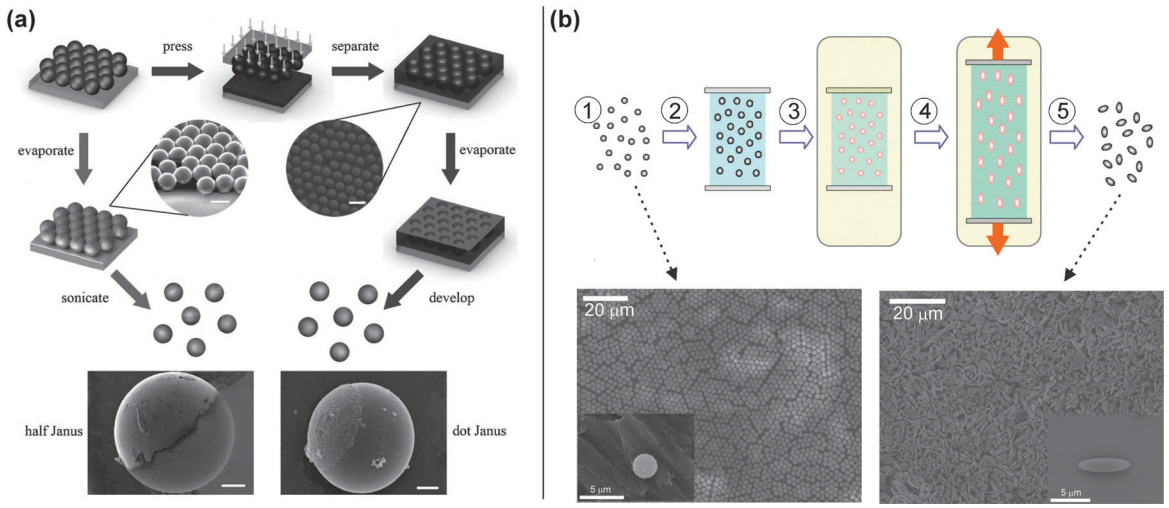

Fig. 4 (a) Schematics (top) showing two methods to fabricate half (left side) and dot (right side) magnetic Janus particles, SEM images at the bottom. (b) Schematics (top) showing the fabrication of paramagnetic microellipsoids. SEM images (bottom) of the pristine colloids (left) and of the resulting ellipsoids (right). [(a) Reprinted with permission from ref. 39 and (b) from ref. 40 (Copyright 2009 and 2010 Wiley)].

the pores determines the rod diameters, while the length of the rods can be controlled by adjusting the deposition time. Finally the metallic rods are recovered by etching the sacrificial membrane. Fig. 5(a_2,a_3) show some multisegmented Ni/Au/Ni nanorods obtained by Hangarter and Myung[46] following a similar procedure.

While the previous method enables to produce long nanowires with a diameter as small as $\sim$5 nm, it does not allows to modify the shape of the rods during growth, *i.e.* to add arms or branches which could provide a further degree of functionality. Soft lithographic techniques can be successfully used for this purpose, although they do not permit the same degree of miniaturization in the produced particles. Fig. 5(b) shows an example of an elongated magnetic microstructure (b_5) realized *via* microtransfer molding.[58] The process is shown in more detail in the sequence of images (b_1–b_4). First, photolithography was used to transfer the motif from a photomask to a SU8 photoresist, which was treated with UV and later developed in propyleneglycol methylethylacrylate in order to dissolve unexposed parts. The mould (b_1) was obtained from a photoresist *via* direct PDMS replica and its cavities were filled with PDMS doped by a ferrite powder (b_2). The polymer was cured thermally in the presence of an external field to magnetize the structure (b_3). Once released from the mold, this magnetic structure was able to propel in water under a rotating magnetic field.[47]

The use of lithographic techniques to produce complex magnetic particles is currently a matter of intense research[59–65] due to the unprecedented flexibility to design apriori any complex structure. Recently, Sakar *et al.*[66] simplified the microfabrication process realizing in a single step ferromagnetic U-shaped microparticles, used to engage and transport a biological cargo. Another example of polymeric microactuators capable of performing several functions has been recently demonstrated by Kim *et al.*[67] These authors realized separate compartments of a solidified photocurable resin characterized by a defined magnetic anisotropy. The anisotropy was given by the orientation of embedded chains of magnetic nanoparticles. The external field generated by a magnet was able to orient these compartments in different directions, allowing simple operations like oscillations, tweezing, or net displacement.

Microfluidic-based synthesis of colloidal microparticles is an alternative strategy which allows high-throughput production of monodisperse colloids using low-volume of starting material. Particles are usually generated by coflowing two immiscible fluids, while temperature or UV light is used to polymerize these fluids directly within the channel. The particle size may be set from the width of the channel, or by varying the relative flow rates during coflow. Kim and co-workers[68] used a capillary-based microfluidic device to produce magnetically doped spherical microgel particles. Anisotropic magnetic hydrogel particles in the form of disks and plugs were produced by Hwang *et al.*[69] employing a T-junction. Fig. 5(c_1) shows the microfluidic device built up by Yuet *et al.*[48] to generate $\sim$50 μm size Janus magnetic colloids (c_2). In this set-up, two flowing mineral oils were used to shear off monodisperse emulsions composed of two photocurable polymers, one doped with magnetite. This technique permitted to encapsulate biological materials as well as to selectively functionalize the particle surface with DNA or different fluorophores. A variant of this technique has been later proposed to produce magnetic Janus particles,[70] Janus supraballs for flexible display,[71] and dimer capsules.[72] Finally, the work of Maeda *et al.*[73] should be also mentioned in which the authors developed a simple approach to generate Janus magnetic colloids *via* controlled centrifugation.

3 Dynamics and assembly

3.1 Magnetically torqued ellipsoid

Under the action of an external field, anisotropic colloids tend to reorient along the field direction. Let us consider the simple case of a paramagnetic ellipsoid, such as the one shown in Fig. 4(b). The ellipsoid displays a preferred magnetization along its long axis, which defines a director $\hat{\mathbf{n}}$. The magnetic susceptibility χ is a scalar for isotropic particles, but becomes a tensor $\bar{\chi}$ for anisotropic ones. For a prolate ellipsoid, it is a second order

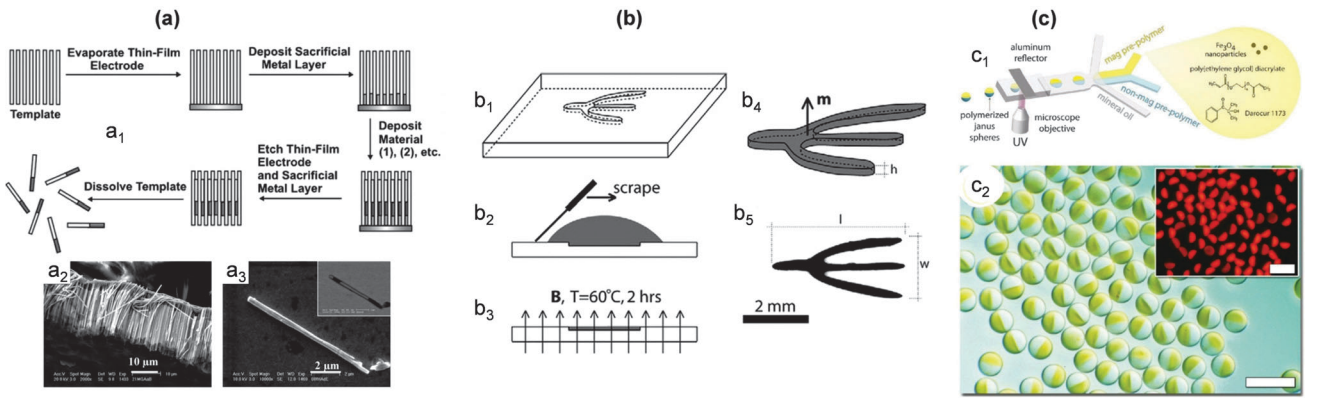

Fig. 5 (a_1) Schematics illustrating the procedure used to grow metallic nanowires. (a_2, a_3) SEM images of segmented Ni/Au/Ni nanowires. Schematics (b_1–b_4) and image (b_5) showing the fabrication of a PDMS magnetic swimmer. (c_1) Flow-focusing device used to fabricate magnetic Janus particles, shown in the brightfield (c_2) and fluorescent (inset) microscope images, scale bars are 100 μm. [(a_1) Reprinted with permission from ref. 45 (Copyright 2006 Wiley), (a_2, a_3) from ref. 46 (Copyright 2005 ACS), (b) from ref. 47 and (c) from ref. 48 (Copyright 2009 ACS)].

tensor which can be written as, $\bar{\chi} = \chi_{\perp}\bar{I} + \Delta\chi\hat{\mathbf{n}}\hat{\mathbf{n}}$ being $\chi_{\parallel}$ and $\chi_{\perp}$ the parallel and perpendicular component with respect to $\hat{\mathbf{n}}$, $\Delta\chi = \chi_{\parallel} - \chi_{\perp}$ and $\bar{I}$ the isotropic tensor.[77] These components are related to the demagnetizing field factors $N_{\parallel}$ and $N_{\perp}$ of the ellipsoids following $\chi_{\parallel,\perp} = \chi_0/(1 + \chi_0 N_{\parallel,\perp})$, with χ_0 being the isotropic intrinsic susceptibility.[78] An external magnetic field $\mathbf{H}$ at an arbitrary angle with respect to $\hat{\mathbf{n}}$ will give a finite torque $\boldsymbol{\tau}_m = \mu_w \mathbf{m} \times \mathbf{H}$, being $\mu_w \sim \mu_0 = 4\pi \times 10^{-7}$ H m^{-1} the magnetic permeability of the dispersing medium (water) and $\mathbf{m} = \bar{\chi} V \mathbf{H}$. the dipole moment. For large ellipsoids, thermal fluctuations can be neglected and the deterministic dynamics is described by a torque balance equation,

$$\boldsymbol{\tau}_m + \boldsymbol{\tau}_v = \mathbf{0} \tag{1}$$

being $\boldsymbol{\tau}_v = -\zeta_r \tilde{\boldsymbol{\omega}}$ the viscous torque arising from the rotation of the ellipsoid in the medium with angular velocity $\tilde{\boldsymbol{\omega}}$, and rotational friction coefficient ζ_r. Solving this equation for a static field enables us to find the angle φ between $\hat{\mathbf{n}}$ and $\mathbf{H}$ as,

$$\varphi(t) = \tan^{-1}\left[\tan(\varphi_0)\exp\left(\frac{t - t_0}{\tau_r}\right)\right] \tag{2}$$

where $\varphi = \varphi_0$ at $t = t_0$, and the relaxation time $\tau_r = \dfrac{3\zeta_r}{4bc^2\pi\mu_w\Delta\chi H^2}$ being $b(c)$ the long (short) semiaxis of the ellipsoid. If the magnetic field rotates in the plane of the particle (x, y) with angular frequency $\omega = 2\pi f$ and amplitude $\hat{H}$, $\mathbf{H} \equiv \hat{H}(\cos(\omega t),\sin(\omega t))$, eqn (1) can be written in term of the phase-lag angle φ as, $\dot{\varphi} = \omega - \omega_c \sin(2\varphi)$ where $\omega_c = (2\tau_r)^{-1}$ is the critical "frequency". The latter equation admits an analytical solution,[79] describing the ellipsoid rotational motion. When $\omega < \omega_c$, the ellipsoid rotates synchronously with the field and the phase-lag angle is constant. For frequencies $\omega > \omega_c$ the ellipsoid shows a characteristic "back-and-forth" motion during each cycle of the applied field. For smaller ellipsoids, when thermal fluctuations become important, the particles exhibit a crossover from anisotropic diffusion, $D_{\parallel} \neq D_{\perp}$ to a long time isotropic one.[2] Here $D_{\parallel}$ and $D_{\perp}$ are the diffusion coefficients related to the translation parallel and perpendicular to the ellipsoid long axis, resp. At longer time, rotational diffusion erases the directional memory of the particle, and the thermal motion can be describe by one diffusion coefficient $\bar{D} = (D_{\parallel} + D_{\perp})/2$. As shown by Güell *et al.*,[80] application of an external field static or time-dependent can be used to increase or decrease respectively the crossover time, and thus to control the particle diffusive dynamics in the fluid medium.

3.2 Magnetic dipolar interactions

Ferromagnetic particles or paramagnetic ones under an external field assemble into elongated structures due to attractive dipolar forces. If one considers an ensemble of dipoles $\mathbf{m}_i$, each dipole will interact with the local field generated by the others. The dipolar interaction between two particles i and j with a center to center distance r is given by,[81]

$$U_d = -\frac{\mu_w}{4\pi}\left(\frac{3(\mathbf{m}_i \cdot \hat{\mathbf{r}})(\mathbf{m}_j \cdot \hat{\mathbf{r}}) - \mathbf{m}_i \cdot \mathbf{m}_j}{r^3}\right) \tag{3}$$

being $\mathbf{r} = \hat{\mathbf{r}}r$. For similar moments $\mathbf{m}_i = \mathbf{m}_j = \mathbf{m}$ aligned along the field, eqn (3) reduces to the relationship, $U_d = -\dfrac{\mu_w m^2}{2\pi r^3}P_2(\cos(\theta))$, with $P_2(x) = \dfrac{1}{2}(3x^2 - 1)$ being the second-order Legendre polynomial, and θ the angle between the dipoles and their line of separation. When $\theta < \theta_m$, $U_d < 0$ the dipoles attract each other, while when $\theta > \theta_m$, $U_d > 0$ they repel, $\theta_m = 54.7^{\circ}$ being the "magic" angle. The force between the two particles can be derived directly from the potential as, and in spherical coordinates becomes:[82]

$$\boldsymbol{F}_d = -\frac{3\mu_w m^2}{2\pi r^4}\left[P_2(\cos(\theta))\hat{\mathbf{r}} + \frac{\sin(2\theta)}{2}\hat{\boldsymbol{\theta}}\right] \tag{4}$$

The chaining effect described in Section 2.2 for isotropic particles follows from the radial component of the force, which tend to align the moments along the common direction $\hat{m} = \hat{H}$. Using eqn (4), one can estimate the aggregation time between a pair of isotropic paramagnetic particles of radius a, both with an induced moment $m = (4/3)\pi a^3 \chi H$, neglecting corrections due to the local dipolar field.[83] The total force between a pair of dipoles at an initial distance r_0 ($t = 0$) is given by $M\ddot{r} = -\gamma\dot{r} + \dfrac{3\mu_w m^2}{\pi r^4}$, with $\gamma = 6\pi\eta a$ being the friction coefficient. Solving this equation after neglecting the inertia term gives an aggregation time $t_a = \dfrac{36\eta}{5H^2\mu_w\chi^2}\left[\left(\dfrac{r_0}{2a}\right)^5 - 1\right]$. For an initial distance of $r_0 = 15$ μm, and under an applied field of $H = 4 \times 10^5$ A m^{-1}, paramagnetic particles of 1 μm diameter, $\chi \sim 0.4$ will require $t_a = 0.17$ s to form a doublet.

3.3 Magnetically assembled structures

Compared to isotropic particles, the assembly of anisotropic ones provides a much richer scenario, due to the competition between magnetic interactions and geometric restrictions. Zerrouki *et al.*[74] studied the chaining process of symmetric and asymmetric dumbbells, characterized by magnetic caps or rings. These colloidal units, shown in the top part of Fig. 6(a), were realized *via* the emulsion confinement method.[84] This technique consisted of encapsulating silica particles having different sizes within droplets of an octane based ferrofluid. Controlled evaporation of the octane forced the packing of the silica colloids into symmetric or asymmetric clusters of doublets depending on the size of the entrapped particles.[85] De-wetting of the ferrofluid on the curved silica surface formed iron-oxide caps above spherical particles, and rings encircling symmetric and asymmetric doublets. As shown in the fourth row of Fig. 6(a), symmetric dumbbells with a magnetic belt assembled into a periodically twisted achiral chain. Chirality was observed for the asymmetric dumbbells, bottom of Fig. 6(a). In this case, the size difference between the individual particles forced the anisotropic units to redistribute into an helical-like structure in order to maximize the alignment of the magnetic rings.

Under a static field, magnetic Janus particles assemble into staggered chains,[48,51,53,86] with magnetic poles facing each other in order to minimize the magnetic energy of the aggregate.

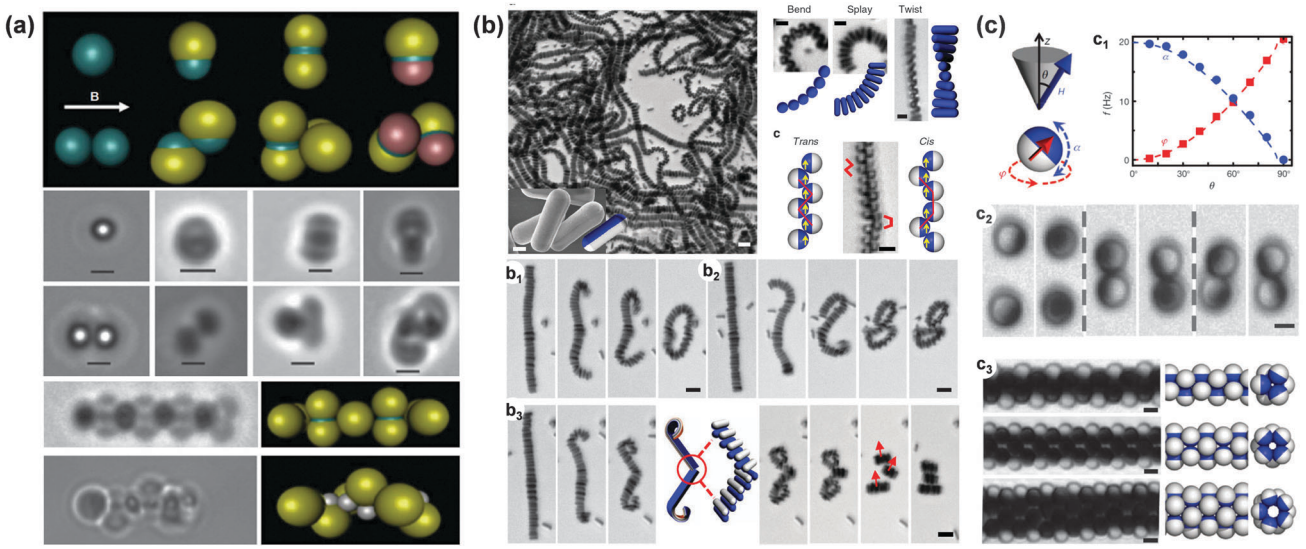

Fig. 6 (a) Schematics (top) and experimental realization (second and third rows) of assemblies of spherical magnetic particles (left) and magnetic dumbbells (right), scale bars are 1 μm. Chains composed of symmetric (fourth row) and asymmetric (fifth row) dumbbells. (b) Top left: self-assembled ribbons of magnetic Janus rods, right: different liquid-crystal like deformations of a colloidal ribbon, scale bar is 2 μm. Bottom rows: formation of one (b_1), two (b_2) or three (b_3) rings from a ribbon by reversing the applied field, scale bar is 4 μm. (c) Schematic showing a magnetic Janus colloid under a precessing magnetic field. (c_1) Oscillation frequencies α and ϕ of the particle *versus* the field precession angle θ. (c_2) Dynamic approach of two magnetic Janus particles under the precessing field. (c_3) Images (left) and schematic from simulation (right) of microtubes formed parallel to the precession axis. [(a) Reprinted with permission from ref. 74, (b) from ref. 75 and (c) from ref. 76 (Copyright 2008, 2013 and 2012 Nature Publishing Group)].

More complex structures composed of anisotropic Janus colloids have been recently reported by Yan *et al.*[75] The magnetic rods in Fig. 6(b) were realized by coating monodisperse silica rods[89] with a Ni layer. Under an external field, the ferromagnetic rods oriented perpendicular to the field direction forming a ribbon, a similar assembly behaviour observed for the hematite particles in Fig. 2(f). The bottom row in Fig. 6(b) shows the evolution of a ribbon towards a low energy ring state upon reversing the direction of the applied field. Three different pathways were possible, where the ends of the ribbon curved in the same direction forming an hairpin (b_1), curved in opposite directions *via* an S-shape deformation (b_2) or, the ribbon fragmented into three dipolar rings when the field was reversed very fast.

While static magnetic fields organize particles into complex although immobile structures, time-dependent fields can be used to generate dynamic assemblies, with a richer collective behaviour.[90,91] Quite recently Yan *et al.*[76] used a precessing magnetic field to assemble Janus colloids into micrometer-scale tubes. A processing field around a particular axis (z-axis in Fig. 6(c)) with a precession angle ϑ can be obtained by combining a static field along this axis, $H_z = \hat{H}\cos\vartheta$ with a rotating one in the perpendicular plane (x, y), $\boldsymbol{H} = \hat{H}(\cos\vartheta\mathbf{e}_z + \sin\vartheta[\cos(\omega t)\boldsymbol{e}_x + \sin(\omega t)\boldsymbol{e}_y])$. Here the amplitudes of the circularly polarized rotating field are $H_x = H_y = \hat{H}\sin\vartheta$. Subjected to the precessing field of constant amplitude $\hat{H} = 4.0$ kA m^{-1}, an individual Janus particle showed angular rotations ($\varphi(t)$) and vertical oscillations ($\alpha(t)$) characterized by a frequency f which could be controlled by the precession angle, Fig. 6(c_1). A pair of approaching particles showed an anti-phase synchronization behaviour, Fig. 6(c_2), with frequency locking resulting from time-averaged attracting dipolar forces. The collective behaviour was remarkable, with particles approaching in the form of zigzag chains and wrapping around creating long hollow microtubes at low precession angle. Fig. 6(c_3) shows three types of such microtubes which developed parallel to the precession axis, and characterized by different elementary stacking of Janus particles, from three to five (top to bottom), having the magnetic caps of the particles facing inward. These dynamic structures were found to be stationary only for a certain region of field parameters, where synchronization occurred between the globally rotating microtube and its oscillating colloidal parts. Larger frequencies or precessing angles destabilized the structures into zigzag chains or planar sheets, due to loss of synchronization and a corresponding structural transition.

4 Applications

4.1 Active microrheology probes

Passive microrheology measures the viscoelastic properties of complex fluids by tracking the Brownian motion of embedded colloidal probes.[92,93] While this technique presents some advantages over conventional rheology, such us the sensitivity and the high range of frequency available, it cannot infer highly viscous materials using thermal fluctuations. Active microrheology on the other hand, uses an external field to induce periodic rotation or displacement of an embedded particle, and measures the corresponding material deformation.[94,95] Active magnetic microrheology, where magnetic particles are driven in a viscoelastic medium, is even older than the "passive" counterpart based on particle-tracking, and date back to the pioneering work of Crick and Hughes on chick fibroblasts.[96] A magnetic bead

microrheometer[97–101] usually employs spherical paramagnetic or ferromagnetic particles subjected to strong and inhomogeneous magnetic fields, allowing to generate a force ranging from 10^{-3} to 10^{2} pN.[102]

The simplest anisotropic probe one can think of is a magnetic rod, which is appealing for study the rheological properties of monolayers at the water/air interface, since rods can be easily absorbed at an interface due to their large aspect ratio. Interfacial viscometers based on macroscopic rods have been developed by several groups,[103–106] but the use of nanometer size probes is quite recent.[107] The main advantage in reducing the probe size is the drastic increase in sensitivity, since it produces an increase in the Boussinesq number (Bo), *i.e.* the ratio between the interface and sub-phase drag, $\mathrm{Bo} \sim \frac{\eta_s}{\eta_b a}$. Here η_s (η_b) is the surface (bulk) viscosity and a is a characteristic length associated with the size of the probe. Nanorods are more sensitive than macroscopic ones since reducing a increases Bo and reduces the coupling between the interfacial flow and the subphase.

In a recent realization, Dhar *et al.*[87] were able to reach a sensitivity of $\eta_s \sim 10^{-9}$ N s m^{-1} using a magnetic nanorod, three orders of magnitude lower than the resolution of macroscopic rods.[108] The nickel nanorod (3 μm in length and 300 nm in diameter) was used to measure the surface viscosity of albumin at different aging times. As shown in Fig. 7(a), the magnetic torque was applied by switching the orientation of an in plane magnetic field H. The orientation angle φ between the rod's long axis and the applied field follows an equation similar to eqn (3), where the relaxation time $\tau_r \propto f_r$, with $f_r = f_w + f_s$ being the sum of the bulk (f_w) and surface (f_s) drag, the latter related to Bo and thus to the surface viscosity.[109] With this technique, it was possible to demonstrate that the surface viscosity of albumin increased significantly with aging compared to the surface pressure, suggesting the annealing with time of the protein film.

Choi *et al.*[88] used ferromagnetic "microbuttons" to measure the surface viscosity of a phospholipid monolayer (DPPC), reaching a resolution of $\eta_s \sim 10^{-8}$ N s m^{-1}. These anisotropic probes (20 μm in diameter) were realized by a photolithographic process using a SU-8 photoresist.[59] An in-plane oscillatory magnetic field was used to rotate these probes. Bright-field and fluorescent microscopy were used to simultaneously visualize the particle motion and the DPPC deformations, Fig. 7(c and e). While a small applied torque induced an elastic response of the DPPC monolayer at low frequencies, a large amplitude deformation forced the creation of a "slip-line" encircling the rotating probe, and generated viscous response at all frequencies, Fig. 7(e and f).

Besides interfacial microrheology, anisotropic probes can also be used for rheological measurements of viscoelasticity in the bulk. In contrast to isotropic particles, anisotropic probes like magnetic rods,[110,111] wires,[112,113] or ellipsoids[114] offer the advantages of requiring a uniform magnetic field to be torqued and corresponding easy visualization. In particular, magnetic rotational microrheology was successfully used to measure the viscoelastic properties of living cells.[115,116]

4.2 Stirring, trapping, and sorting

An elongated particle torqued by an external rotating field generates a hydrodynamic vertical flow and thus can be used as a microscopic analog of a magnetic stir bar. Due to the laminar nature of fluid flow at low Reynolds number (Re), the

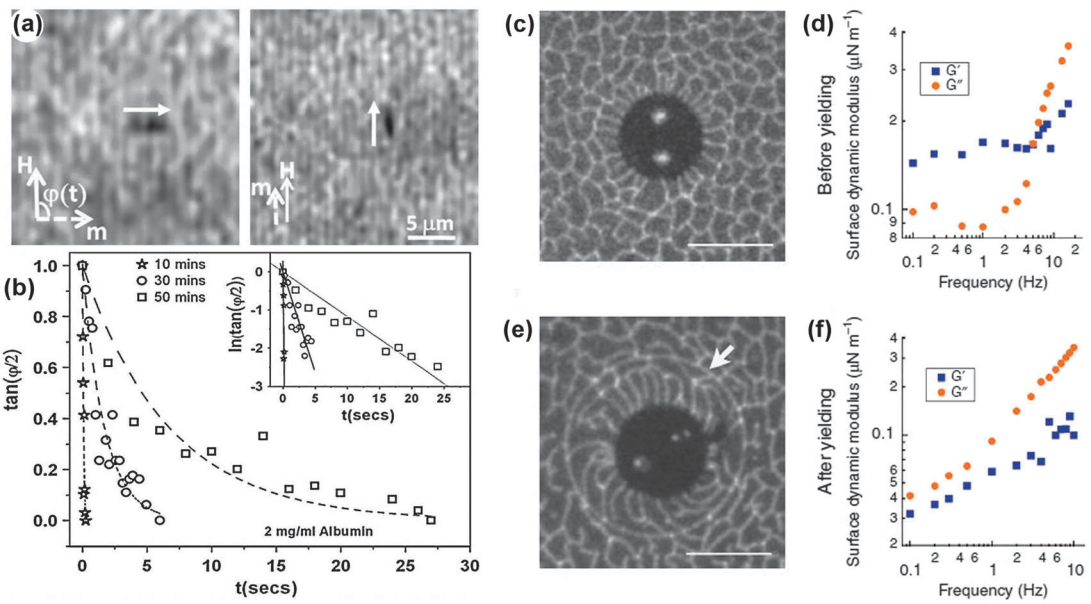

Fig. 7 (a) Orientation of a magnetic nanorod under a static field in a solution of albumin. (b) tan(φ/2) *versus* t at different aging times. (c, e) Ferromagnetic "microbutton" rotating in a dipalmitoylphosphatidylcholine monolayer for small (c) and strong (e) deformations. (d, f) Surface shear moduli (elastic $G'(\omega)$, viscous $G''(\omega)$) before (d) and after (f) yielding. [(a, b) Reprinted with permission from ref. 87 (Copyright 2010 APS), (c–f) from ref. 88 (Copyright 2011 Nature Publishing Group)].

efficiency of this "microstirrer" is strongly reduced. For a rotating stirrer, $\mathrm{Re} = \frac{\rho v l}{\mu}$ gives the ratio between "inertial" and viscous force, with v and l being the characteristic velocity and length scales resp., and $\rho(\mu)$ the density (dynamic viscosity) of the dispersing medium. For a magnetic microrod rotating around its 1 μm long axis at an angular speed of $\tilde{\omega} = 50\ \mathrm{s}^{-1}$ in water ($\nu = \mu/\rho = 10^{-3}\ \mathrm{m}^2\ \mathrm{s}^{-1}$) $\mathrm{Re} = \frac{\tilde{\omega} a^2}{\nu} = 10^{-8}$, *i.e.* several orders of magnitude lower than the corresponding value for a $a = 2.5$ cm long stir bar, $\mathrm{Re} = 3 \times 10^4$.[119] However in constrained geometries such us in a microfluidic channel, colloidal inclusions can be effectively used to displace fluids or to perform simple operations.[120] In particular, isotropic paramagnetic colloids dynamically assembled by a rotating magnetic field into anisotropic clusters[121] have been successfully implemented as "active" pumping elements in soft-lithographic channels.[122,123]

Apart from microfluidic systems, rotating anisotropic particles find applications in microscale trapping or sorting based on hydrodynamic or magnetic interactions. The hydrodynamic "trapping" capability of rotating nickel nanowires was recently demonstrated by Petit *et al.*[117] The nanowires (15 μm long with ~200 nm diameter) were synthesized by electrochemical deposition in an aluminium oxide template. Low intense ($H \sim 2\ \mathrm{kA\ m}^{-1}$) rotating fields were used to spin the nanowires, and passive microspheres or bacteria were trapped by the generated flow field. As shown in Fig. 8(a and b), the flow velocity profile generated by the microvortices was characterized by a local minima close to the center of the nanowire. In Fig. 8(c) are a series of images in a row showing how the authors used his concept to transport (second images of the sequence), trap (third image) and release (fourth image) a 6 μm size PSt microsphere.

In contrast to high-aspect ratio nanowires, the DNA linked anisotropic doublets shown in Fig. 3(a), were unable to generate a strong hydrodynamic flow. However their magnetic anisotropy allowed us to induce complex interactions between the particles, leading to sorting for certain field parameters. Fig. 8(d) shows a schematic of two interacting doublets spinning due to a precessing magnetic field, with frequency Ω and precession angle ϑ. The different behaviour between isotropic (spherical) and anisotropic (doublets) rotors is highlighted in Fig. 8(e) for a constant field amplitude $H = 1.3\ \mathrm{kA\ m}^{-1}$, and varying Ω and ϑ. Isotropic rotors were well described by dipolar coupling, repelling (attracting) for $\vartheta < \vartheta_m$ ($\vartheta < \vartheta_m$), with ϑ_m being the magic angle. The anisotropic rotors in contrast, repelled also for angles $\vartheta_m < \vartheta < 61.5°$. This stronger repulsive behaviour was due to the presence of nonzero higher magnetic multipole moments. In particular, close to the magic angle, when the dipole–dipole term becomes small, the particles repelled *via* dipole–hexapole interactions.[118] The sequence of images in Fig. 8(f–h), shows how this feature was used to discriminate between the two types of rotors close to ϑ_m. For precession angle $\vartheta = 0°$ (f), repulsive dipolar interactions separated all type of rotors, colloidal doublets (blue arrows) and isotropic spheres (green arrows). In (g) the precession angle was switched to $\vartheta = 56.7°$ in order to separate the doublets from the spheres which collapsed after $t = 14.5$ s (h).

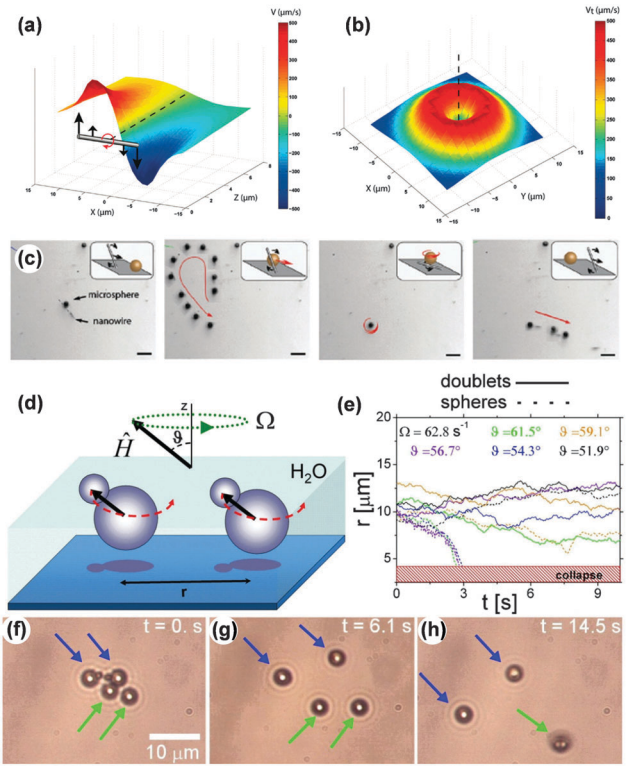

Fig. 8 (a) Flow velocity profile induced by a rotating nanowire and (b) averaged tangential flow velocity, both images from numerical simulations. (c) Microscope images showing the manipulation of a PSt microsphere. (d) Schematic showing two rotating interacting doublets. (e) Distances r *vs.* time t for doublets (continuous lines) and isotropic particles (dashed lines). (f) Sorting of paramagnetic doublets but not particles. [(a–c) Reprinted with permission from ref. 117 and (d–h) from ref. 118 (Copyright 2012 and 2009 ACS)].

4.3 Magnetically driven propellers

Anisotropic particles can be propelled in a fluid medium when a proper strategy is developed to take into account the negligible role of inertia at low Re. Under these conditions, particles displaying reciprocal motion, *i.e.* symmetric backward and forward body distortions, are unable to move.[124] Thus, a magnetic rod or an ellipsoid immersed in a bulk fluid and torqued by a uniform rotating field, will rotate but not translate, independently on the frequency or amplitude used.

There are different ways to break the time reversible symmetry of the fluid flow at low Re, and generate net motion. Fig. 9 shows most of the magnetic propellers recently realized, with the actuating field displayed in the middle column. Common features are the use of a magnetic field which is uniform and time dependent, such that the net particle motion does not result from the presence of a gradient, but rather arises from a rectification process, where oscillations or rotations are transformed into direct motion. There are mainly three strategies which have been successfully used:[125,126] (i) flexibility in the

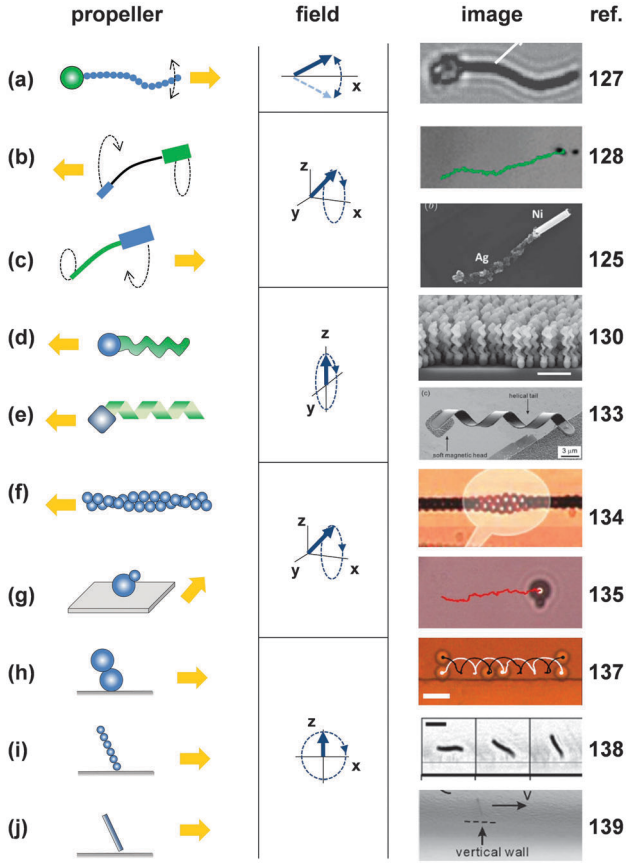

Fig. 9 Schematics and images of magnetic propellers based on anisotropic magnetic colloids. The first column shows a cartoon of the propeller with the direction of motion, the second column the applied field, the third one an experimental image, and the corresponding reference on the right side of the image.

colloidal unit, Fig. 9(a–c), (ii) helicity in the shape, Fig. 9(d–f) or (iii) close proximity to a boundary, Fig. 9(g–j).

Fig. 9(a) shows a colloidal microswimmer composed of a flexible magnetic filament (~30 μm long) of 1 μm size DNA-linked paramagnetic colloids attached to a ~3 μm red-blood cell.[127] Non-reciprocal beating movements of the magnetic tail were induced by an oscillating magnetic field, $\boldsymbol{H} \equiv (H_x, H_y \sin \omega t, 0)$. The symmetry was broken by the presence of the cargo, which was carried up to a maximum speed of v_{max} = 22 μm s^{-1} for field strengths of H_x = 7.0 kA m^{-1}, H_y = 8.0 kA m^{-1} and f = 10 Hz.[127] Flexibility was also used by Gao *et al.*[128] and by Pak *et al.*[125] to propel magnetic nanowires composed of three (Au, Ag, Ni) and two (Ag, Ni) metallic segments, respectively. Both types of propellers were fabricated *via* template-assisted electrodeposition, and presented a total length of ~6 μm and 200 nm in diameter. The flexibility was provided by the Ag segment, which was partially dissolved in an hydrogen peroxide (H_2O_2) solution before the experiments. An external precessing magnetic field was used to deform these nanowires in a chiral fashion in order to obtain a net motion. In particular, the Ag/Ni propeller result to be the faster, reaching a maximum speed v_m = 21 μm s^{-1} for $\hat{H} \sim$ 1.4 kA m^{-1}, $\vartheta = 35°$ and f = 35 Hz (v_m = 6 μm s^{-1} for the striped Au/Ag/Ni for $\hat{H} \sim$ 0.4 kA m^{-1} and f = 15 Hz),[125] and was later successfully employed in docking and delivery operations of microscopic cargos.[129]

Similar to the flagellum of the bacterium *E.coli*, a rotating helical tail is capable of propelling in a viscous fluid. Fig. 9(d–f) show three bio-inspired examples. The silica propellers in (d) were fabricated *via* a glancing angle deposition method, and after being released from the substrate, were covered by a thin Co layer *via* thermal evaporation of the metal.[130,131] An alternative method to engineer the helical structures was developed by Zhang *et al.*[132,133] The artificial flagellum shown in row (e) was realized *via* self-scrolling of a nanobelt made by semiconductor–metal layers, and terminated in a soft-magnetic head containing Ni. Both types of propellers were moved in a fluid *via* an external rotating field, reaching a speed as high as v_m = 40 μm s^{-1} ($\hat{H}$ = 4.8 kA m^{-1}, f = 150 Hz) for the silica propeller, and v_m = 18 μm s^{-1} ($\hat{H}$ = 1.6 kA m^{-1}, f = 30 Hz) for the other one. Shown in row (f) is a dynamic helical structure developed by Casic *et al.*[134] and composed of isotropic particles assembled *via* time averaged attractive dipolar interactions. The ribbon assumed a chiral conformation *via* traveling twist walls, when subjected to an elliptically precessing magnetic field. Although the average translational speed of this dynamic propeller was smaller compared to other prototypes, v_m = 0.6 μm s^{-1} ($\hat{H}$ = 2.2 kA m^{-1}, f = 23 Hz) the traveling walls along the chains add further functionality, including for example transport of nonmagnetic cargo by mobile twist walls.

The rest of the propellers shown in Fig. 9 used the proximity of a wall to rectify their rotational motion into a net translation. Besides the asymmetric doublets in row (g) which required a precessing field,[135,136] symmetric doublets[137] (h), chains[138] (i) and rods[139] (j) were all propelled by a circularly polarized rotating field. In all cases, the direction of motion of the propeller was dictated by the sense of rotation of the field, and the average speed linearly increased with the driving frequency up to a certain threshold value, after which the propeller loosed the phase with the field. The asymmetric doublets were slower[140] (v_m = 3.2 μm s^{-1} for $\hat{H}$ = 4.2 kA m^{-1}, $\vartheta = 72°$, f = 15 Hz) compared to longer aggregates, although their speed could be improved by using an attractive magnetic substrate, such as the case of the symmetric doublets in (h). On the other hand, for longer aggregates it was found that chains with intermediate length (3–4 particles) were faster with v_m = 12 μm s^{-1} (for $\hat{H} \sim$ 3 kA m^{-1}, f = 32 Hz) compared to longer ones (7 particles). This behaviour resulted from the increase of the rotational friction coefficient with the length, which induced fragmentation of the rotating chains.[138] Stiff magnetic wires having 12 μm length were able to reach v_m = 37 μm s^{-1} (for $\hat{H} \sim$ 2.6 kA m^{-1}, f = 34 Hz) before loosing the phase with the driving field.

4.4 Magnetically controlled propellers

When propulsion arises from a different mechanism, like a chemical reaction,[143–145] external fields can be used to orient and steer propellers containing magnetic parts. Control over directionality of a microppropeller is important for applications related with precise and fast docking of chemical or

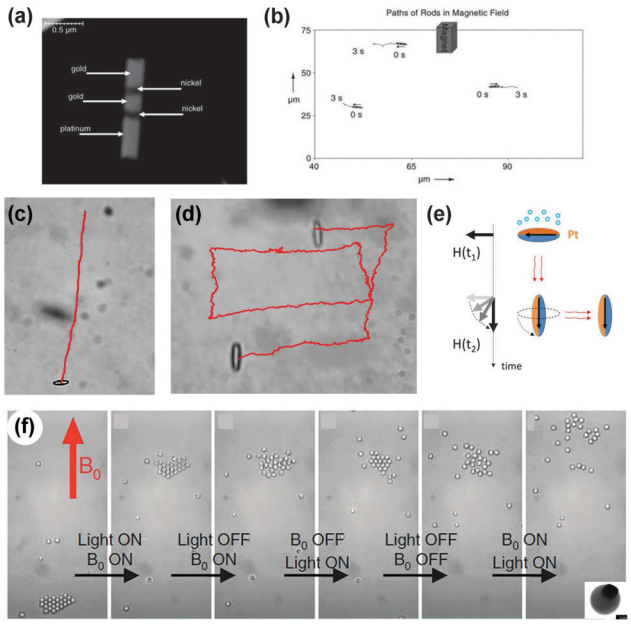

Fig. 10 (a) SEM image of a striped metallic nanorod composed of five segments, Au/Ni/Au/Ni/Pt. (b) Trajectories of the nanorods in an aqueous H_2O_2 solution and under a static magnetic field. (c–e) Magnetically guided motion of paramagnetic microellipsoids half coated with Pt in aqueous H_2O_2 solution. (f) Sequence of images showing the magnetic control of colloidal surfers, with an individual unit shown in the inset (bottom-left). [(a, b) Reprinted with permission from ref. 141 and (c–e) from ref. 40 (Copyright 2005 and 2010 Wiley); (f) from ref. 142 (Copyright 2013 AAAS)].

biological cargos. As an example of an autonomous moving propeller, one can consider the case of a 2 μm long Pt/Au nanorod in a H_2O_2 aqueous solution.[144] The Pt part catalyzes the decomposition of H_2O_2 in water ($2H_2O_2 \rightarrow O_2(g) + 2H_2O(l)$) and propulsion arises due to an interfacial tension gradient generated by this reaction. In the absence of an effective steering mechanism, the rod trajectory undergoes random deflections from its original path, due to thermal fluctuations or to an unequal distribution of the reacting chemicals. To gain complete control over the particle trajectory, Kline *et al.*[141] realized a multi-component striped rod, composed of two Ni segments sandwiched between two Au parts and a Ni one, Fig. 10(a). The Ni parts were initially magnetized perpendicular to the rod long axis, and the propeller was guided in an aqueous H_2O_2 by orienting an external magnet, as shown in Fig. 10(b).

Rotational diffusion also strongly affects the directionality of Janus particles propelling in an aqueous H_2O_2 solution.[146,147] Making a spherical propeller responsive to an external field in order to guide its motion can be done in different ways, like by evaporating a metallic cap on top of it,[148] or by replacing the pristine particle with a magnetic one.[40] The latter case is illustrated in Fig. 10(c–e), where paramagnetic microellipsoids covered by a Pt layer were propelled in aqueous H_2O_2 solution. Fig. 10(e) shows the basic mechanism: a static field $H = 0.8$ kA m^{-1} torqued the ellipsoid aligning its magnetic moment m (see Section 3.1), and forced the particle to move into a straight trajectory. To change the particle path, the field was rotated by an arbitrary angle, and the magnetic torque reoriented the moving particle, Fig. 10(d). The same strategy was applied to spherical paramagnetic particles, and it was found that magnetic anisotropy was a necessary ingredient to obtain a net steering mechanism.[40]

An example of collective magnetic guidance was recently reported by Palacci *et al.*[142] and it is shown in Fig. 10(f). The propelling units were polymer spheres with a protruding hematite cube. These colloidal "surfers" were observed to move in aqueous H_2O_2 solution under the action of blue-violet light. At these wavelengths, the light triggered the decomposition of H_2O_2 at the surface of the hematite particles and, when facing this surface close to the substrate, the composite particles started sliding above the generated osmotic flow. Using a static external field $H = 0.8$ kA m^{-1}, the authors were able to guide clusters spontaneously formed *via* phoretic attraction on a defined direction. As shown in the sequence of images in Fig. 10(f), the external field also strengthens the particle interactions, avoiding reorientation effects due to rotational diffusion, which could lead to cluster disaggregation.

External magnetic fields have been recently used to guide the motion of many other propellers, besides the examples shown in Fig. 10, such us rolled-up microtubular jets,[149,150] bubble-ejecting nanotubes,[151] ultrasound-powered nanowires,[152] catalytically propelled nanowires[153] and hematite peanuts.[154] The advantage of magnetic guidance relies on the non-invasive nature of the applied field, which does not perturb the chemical reaction leading to propulsion, as would be the case for an electric field for instance.

5 Conclusions

This article presented an overview of several experimental works based on the realization, assembly and practical applications of anisotropic magnetic colloids, specially focusing on monodisperse particles with microscale size, which can be easily visualized *via* conventional optical microscopy. This multidisciplinary field of research embraces different communities interested in the particle synthesis, interactions, dynamics and practical implementation in lab-on-a-chip devices. Besides the variety of works published on the subject, the field still reserves a number of open directions and future challenges. A next natural step towards basic research is to explore the rich collective dynamics of anisotropic magnetic particles when subjected to time dependent magnetic fields. While recently the attention focused on structures formed by Janus particles,[76] ensembles of interacting ellipsoids, disks, chains, wires or driven swimmers still offer a rich scenario for non-equilibrium dynamics which can give rise to complex phases and emergent behaviours. On the application side, anisotropic particles which can be easily torqued by an external field seek direct implementation in microfluidic devices such as stirrers, valves, pumps or can be used as high resolution microscopic probes for viscoelastic matter.

Acknowledgements

This work was supported by the European Research Council *via* Starting Grant Dynamo (Proj. no. 335040) and by the programs RYC-2011-07605 and FIS2011-15948-E.

References

1 F. Vereda, J. de Vicente and R. Hidalgo-lvarez, *ChemPhysChem*, 2009, **10**, 1165–1179.
2 Y. Han, A. M. Alsayed, M. Nobili, J. Zhang, T. C. Lubensky and A. G. Yodh, *Science*, 2006, **314**, 626–630.
3 J. P. K. Doye, A. A. Louis, I.-C. Lin, L. R. Allen, E. G. Noya, A. W. Wilber, H. C. Koke and R. Lyuse, *Phys. Chem. Chem. Phys.*, 2007, **9**, 2197–2205.
4 K. Zhao and T. G. Mason, *Phys. Rev. Lett.*, 2009, **103**, 208302.
5 Z. Zheng, F. Wang and Y. Han, *Phys. Rev. Lett.*, 2011, **107**, 065702.
6 J. C. Crocker and D. G. Grier, *J. Colloid Interface Sci.*, 1996, **179**, 298–310.
7 E. Matijević, *Annu. Rev. Mater. Sci.*, 1993, **15**, 483–516.
8 M. Haruta and B. Delmon, *J. Chim. Phys. Phys.-Chim. Biol.*, 1986, **83**, 859–868.
9 T. Sugimoto, *Adv. Colloid Interface Sci.*, 1987, **28**, 65–108.
10 E. Matijevic, *Chem. Mater.*, 1993, **5**, 412–426.
11 U. Jeong, X. Teng, Y. Wang, H. Yang and Y. Xia, *Adv. Mater.*, 2007, **19**, 33–60.
12 Y. Wang, X. Su, P. Ding, S. Lu and H. Yu, *Langmuir*, 2013, **29**, 11575–11581.
13 S. H. Lee and C. M. Liddell, *Small*, 2009, **5**, 1957–1962.
14 J. Ge, Y. Hu, T. Zhang and Y. Yin, *J. Am. Chem. Soc.*, 2007, **129**, 8974–8975.
15 A. Okada, D. Nagao, T. Ueno, H. Ishii and M. Konno, *Langmuir*, 2013, **29**, 9004–9009.
16 E. Matijević, R. S. Sapieszko and J. B. Melville, *J. Colloid Interface Sci.*, 1975, **50**, 567–581.
17 T. Sugimoto, M. M. Khan and M. Muramatsu, *Colloids Surf., A*, 1993, **70**, 167.
18 T. Sugimoto, *Monodispersed Particles*, Elsevier, Amsterdam, 2001.
19 S. H. Lee, S. J. Gerbode, B. S. John, F. A. Escobedo, I. Cohen and C. M. Liddell, *J. Mater. Chem.*, 2008, **18**, 4912–4916.
20 L. Rossi, S. Sacanna, W. T. M. Irvine, P. M. Chaikin, D. J. Pine and A. P. Philipse, *Soft Matter*, 2011, **7**, 4139–4142.
21 C. G. Shull, W. A. Strauser and E. O. Wollan, *Phys. Rev.*, 1951, **83**, 333–345.
22 M. V. Mansilla, R. Zysler, D. Fiorani and L. Suber, *Physica B*, 2002, **320**, 206–209.
23 M. Nishi, D. Nagao, K. Hayasaka, H. Ishii and M. Konno, *Soft Matter*, 2012, **8**, 11152–11155.
24 D. Nagao, C. M. van Kats, K. Hayasaka, M. Sugimoto, M. Konno, A. Imhof and A. van Blaaderen, *Langmuir*, 2010, **26**, 5208–5212.
25 S. L. Biswal and A. P. G. AP, *Anal. Chem.*, 2004, **76**, 6448–6455.
26 R. Calhoun, A. Yadav, P. Phelan, A. Vuppu, A. Garcia and M. Hayes, *Lab Chip*, 2006, **76**, 247–257.
27 M. Vilfan, A. Potocvnik, B. Kavcic, N. Osterman, I. Poberaj, A. Vilfan and D. Babic, *Proc. Natl. Acad. Sci. U. S. A.*, 2010, **107**, 1844–1847.
28 N. Coq, A. Bricard, F.-D. Delapierre, L. Malaquin, O. du Roure, M. Fermigier and D. Bartolo, *Phys. Rev. Lett.*, 2011, **107**, 014501.
29 A. Cebers, *J. Phys.: Condens. Matter*, 2003, **15**, S1335–S1344.
30 A. Cebers, *Curr. Opin. Colloid Interface Sci.*, 2005, **10**, 167–175.
31 N. Casic, S. Schreiber, P. Tierno, W. Zimmermann and T. M. Fischer, *Europhys. Lett.*, 2010, **90**, 58001.
32 E. M. Furst, C. Suzuki, M. Fermigier and A. P. Gast, *Langmuir*, 1998, **14**, 7334.
33 J. Philipyx, O. Mondain-Monvalz, F. L. Calderonz and J. Bibette, *J. Phys. D: Appl. Phys.*, 1997, **30**, 2798.
34 L. Cohen-Tannoudji, E. Bertrand, L. Bressy, C. Goubault, J. Baudry, J. Klein, J.-F. Joanny and J. Bibette, *Phys. Rev. Lett.*, 2005, **94**, 038301.
35 P. Tierno, S. V. Reddy, M. G. Roper, T. H. Johansen and T. M. Fischer, *J. Phys. Chem. B*, 2008, **112**, 3833.
36 C. Goubault, P. Jop, M. Fermigier, J. Baudry, E. Bertrand and J. Bibette, *Phys. Rev. Lett.*, 2003, **91**, 260802.
37 S. L. Biswal and A. P. Gast, *Phys. Rev. E: Stat. Phys., Plasmas, Fluids, Relat. Interdiscip. Top.*, 2003, **68**, 021402.
38 Y. Hu, L. He and Y. Yin, *Angew. Chem., Int. Ed.*, 2011, **50**, 3747.
39 R. M. Erb, N. J. Jenness, R. L. Clark and B. B. Yellen, *Adv. Mater.*, 2009, **21**, 4825.
40 P. Tierno, R. Albalat and F. Sagués, *Small*, 2010, **6**, 1749–1752.
41 D. Li, S. Banon and S. L. Biswal, *Soft Matter*, 2010, **6**, 4197.
42 P. Tierno and W. A. Goedel, *J. Phys. Chem. B*, 2006, **110**, 3043–3050.
43 H. W. Duan, D. Y. Wang, M. G. N. S. Sobal, D. G. Kurth and H. Mohwald, *Nano Lett.*, 2005, **5**, 949–952.
44 M. Albrecht, G. Hu, I. L. Guhr, T. C. Ulbrich, J. Boneberg, P. Leiderer and G. Schatz, *Nat. Mater.*, 2005, **4**, 203–206.
45 S. J. Hurst, E. K. Payne, L. Qin and C. A. Mirkin, *Angew. Chem., Int. Ed.*, 2006, **45**, 2672–2692.
46 C. M. Hangarter and N. V. Myung, *Chem. Mater.*, 2005, **17**, 1320–1324.
47 P. Garstecki, P. Tierno, D. B. Weibel, F. Sagués and G. M. Whitesides, *J. Phys.: Condens. Matter*, 2009, **21**, 204110–204118.
48 K. P. Yuet, D. K. Hwang, R. Haghgooie and P. S. Doyle, *Langmuir*, 2010, **26**, 4281–4287.
49 S. Jiang, Q. Chen, M. Tripathy, E. Luijten, K. S. Schweizer and S. Granick, *Adv. Mater.*, 2010, **22**, 1060–1071.
50 A. Walther and A. H. E. Müller, *Chem. Rev.*, 2013, **113**, 5194–5261.
51 S. K. Smoukov, S. Gangwal, M. Marquez and O. D. Velev, *Soft Matter*, 2009, **5**, 1285–1292.
52 I. Sinn, P. Kinnunen, S. N. Pei, R. Clarke, B. H. McNaughton and R. Kopelman, *Appl. Phys. Lett.*, 2011, **98**, 024101.

53 A. K. F. Dyab, M. Ozmen, M. Ersoz and V. N. Paunov, *J. Mater. Chem.*, 2009, **19**, 3475–3481.
54 B. M. Teo, S. K. Suh, T. A. Hatton, M. Ashokkumar and F. Grieser, *Langmuir*, 2011, **27**, 30–33.
55 C. C. Ho, A. Keller, J. A. Odell and R. H. Ottewill, *Colloid Polym. Sci.*, 1993, **271**, 469–479.
56 L. Gabrielson and M. J. Folkes, *J. Mater. Sci.*, 2001, **36**, 1.
57 O. Güell, F. Sagués and P. Tierno, *Adv. Mater.*, 2011, **23**, 3674–3679.
58 X.-M. Zhao, Y. Xia and G. M. Whitesides, *Adv. Mater.*, 1996, **8**, 837–840.
59 S. Q. Choi, S. G. Jang, A. J. Pascall, M. D. Dimitriou, T. Kang, C. J. Hawker and T. M. Squires, *Adv. Mater.*, 2011, **23**, 2348–2352.
60 J. W. Tavacoli, P. Baër, M. Fermigier, D. Bartolo, J. Heuvingh and O. du Roure, *Soft Matter*, 2013, **9**, 9103–9110.
61 S. Y. Lee and S. Yang, *Angew. Chem., Int. Ed.*, 2013, **52**, 8160–8164.
62 H. Li, T. J. Flynn, J. C. Nation, J. Kershaw, L. S. Stephens and C. A. Trinkle, *J. Micromech. Microeng.*, 2013, **23**, 065002.
63 P. K. Shah, M. R. Hughes, Y. Wang, C. E. Sims and N. L. Allbritton, *J. Micromech. Microeng.*, 2013, **23**, 107002.
64 C. W. Shields IV, S. Zhu, Y. Yang, B. Bharti, J. Liu, B. B. Yellen, O. D. Velev and G. P. Lopez, *Soft Matter*, 2013, **9**, 9219–9229.
65 Y. L. Lyubarskaya and A. A. Shestopalov, *ACS Appl. Mater. Interfaces*, 2013, **5**, 7323–7329.
66 M. S. Sakar, E. B. Steager, D. H. Kim, M. J. Kim, G. J. Pappas and V. Kumar, *Appl. Phys. Lett.*, 2010, **96**, 043705.
67 J. Kim, S. E. Chung, S.-E. Choi, H. Lee, J. Kim and S. Kwon, *Nat. Mater.*, 2011, **10**, 747–752.
68 J.-W. Kim, A. S. Utada, A. Fernandez-Nieves, Z. Hu and D. A. Weitz, *Angew. Chem., Int. Ed.*, 2007, **46**, 1819–1822.
69 D. K. Hwang, D. Dendukuri and P. S. Doyle, *Lab Chip*, 2008, **8**, 1640–1647.
70 S.-H. Kim, J. Y. Sim, J.-M. Lim and S.-M. Yang, *Angew. Chem., Int. Ed.*, 2010, **49**, 3786–3790.
71 S.-N. Yin, C.-F. Wang, Z.-Y. Yu, J. Wang, S.-S. Liu and S. Chen, *Adv. Mater.*, 2011, **23**, 2915–2919.
72 A. X. Lu, K. Jiang, D. L. DeVoe and S. R. Raghavan, *Langmuir*, 2013, **23**, 13624–13629.
73 K. Maeda, H. Onoe, M. Takinoue and S. Takeuchi, *Adv. Mater.*, 2012, **24**, 1340–1346.
74 D. Zerrouki, J. Baudry, D. Pine, P. Chaikin and J. Bibette, *Nature*, 2008, **455**, 380.
75 J. Yan, K. Chaudhary, S. C. Bae, J. A. Lewis and S. Granick, *Nat. Commun.*, 2013, **4**, 1516.
76 J. Yan, M. Bloom, S. C. Bae, E. Luijten and S. Granick, *Nature*, 2012, **578**, 491.
77 P. Tierno, J. Claret, F. Sagués and A. Cebers, *Phys. Rev. E: Stat. Phys., Plasmas, Fluids, Relat. Interdiscip. Top.*, 2009, **79**, 021501.
78 J. Cimurs and A. Cebers, *Phys. Rev. E: Stat. Phys., Plasmas, Fluids, Relat. Interdiscip. Top.*, 2013, **87**, 062318.
79 K. Erglis, Q. Wen, V. Ose, A. Zeltins, A. Sharipo, P. Janmey and A. Cebers, *Biophys. J.*, 2007, **93**, 1402.
80 O. Güell, P. Tierno and F. Sagués, *Eur. Phys. J.: Spec. Top.*, 2010, **187**, 15–20.
81 R. E. Rosensweig, *Ferrohydrodynamics*, Cambridge University Press, Cambridge, 1985.
82 J. E. Martin, *Phys. Rev. E: Stat. Phys., Plasmas, Fluids, Relat. Interdiscip. Top.*, 2009, **79**, 011503.
83 H. Zhang and M. Widom, *Phys. Rev. E: Stat. Phys., Plasmas, Fluids, Relat. Interdiscip. Top.*, 1995, **51**, 2099.
84 V. N. Manoharan, M. T. Elsesser and D. J. Pine, *Science*, 2008, **301**, 483–487.
85 D. Zerrouki, B. Rotenberg, S. Abramson, J. Baudry, C. Goubault, F. Leal-Calderon, D. J. Pine and J. Bibette, *Langmuir*, 2006, **22**, 57–62.
86 B. Ren, A. Ruditskiy, J. H. K. Song and I. Kretzschmar, *Langmuir*, 2012, **28**, 1149–1156.
87 P. Dhar, Y. Cao, T. M. Fischer and J. A. Zasadzinski, *Phys. Rev. Lett.*, 2010, **104**, 016001.
88 S. Q. Choi, S. Steltenkamp, J. Zasadzinski and T. M. Squires, *Nat. Commun.*, 2011, **2**, 1–6.
89 A. Kuijk, A. van Blaaderen and A. Imhof, *J. Am. Chem. Soc.*, 2011, **133**, 2346–2349.
90 J. Dobnikar, A. Snezhko and A. Yethiraj, *Soft Matter*, 2013, **9**, 3693.
91 J. E. Martin and A. Snezhko, *Rep. Prog. Phys.*, 2013, **76**, 126601.
92 T. G. Mason and D. A. Weitz, *Phys. Rev. Lett.*, 1995, **74**, 1250–1255.
93 T. M. Squires and T. G. Mason, *Annu. Rev. Fluid Mech.*, 2010, **44**, 413–438.
94 D. Mizuno, D. A. Head, F. C. MacKintosh and C. F. Schmidt, *Macromolecules*, 2008, **41**, 7194–7202.
95 L. G. Wilsonw and W. C. K. Poon, *Phys. Chem. Chem. Phys.*, 2011, **13**, 10617–10630.
96 F. H. C. Crick and A. F. W. Hughes, *Exp. Cell Res.*, 1949, **1**, 37–80.
97 A. R. Bausch, F. Ziemann, A. A. Boulbitch, K. Jacobson and E. Sackmann, *Biophys. J.*, 1998, **75**, 2038–2049.
98 C. Haber and D. Wirtz, *Rev. Sci. Instrum.*, 2000, **71**, 4561–4570.
99 M. Keller, J. Schilling and E. Sackmann, *Rev. Sci. Instrum.*, 2001, **72**, 3626.
100 C. Gosse and V. Croquette, *Biophys. J.*, 2002, **82**, 3314–3329.
101 A. H. B. de Vries, B. E. Krenn, R. van Driel and J. S. Kanger, *Biophys. J.*, 2005, **88**, 2137–2214.
102 K. C. Neuman and A. Nagy, *Nat. Methods*, 2008, **5**, 491–505.
103 R. S. Ghaskadvi, J. B. Ketterson, R. C. MacDonald and P. Dutta, *Rev. Sci. Instrum.*, 1996, **68**, 1792.
104 C. F. Brooks, G. G. Fuller, C. W. Frank and C. R. Robertson, *Langmuir*, 1999, **15**, 2450–2459.
105 J. Ding, H. E. Warriner, J. A. Zasadzinski and D. K. Schwartz, *Langmuir*, 2002, **18**, 2800–2806.
106 G. B. Bantchev and D. K. Schwartz, *Langmuir*, 2003, **19**, 2673–2682.
107 A. Anguelouch, R. L. Leheny and D. H. Reich, *Appl. Phys. Lett.*, 2006, **89**, 111914.
108 S. Reynaert, C. F. Brooks, P. Moldenaers, J. Vermant and G. G. Fuller, *J. Rheol.*, 2008, **52**, 261.

109 P. Dhar, T. M. Fischer, Y. Wang, T. E. Mallouk, W. F. Paxton and A. Sen, *Nano Lett.*, 2006, **6**, 66–72.
110 P. Bender, A. Tschöpe and R. Birringer, *J. Magn. Magn. Mater.*, 2013, **346**, 152–160.
111 R. Colin, L. Chevry, J.-F. Berret and B. Abou, *Soft Matter*, 2014, **10**, 1167–1173.
112 L. Chevry, N. K. Sampathkumar, A. Cebers and J.-F. Berret, *Phys. Rev. E: Stat. Phys., Plasmas, Fluids, Relat. Interdiscip. Top.*, 2013, **88**, 062306.
113 L. Chevry, R. Colin, B. Abou and J.-F. Berret, *Biomaterials*, 2013, **33**, 6299–6305.
114 S. Hernández-Navarro, P. Tierno, J. Ignés-Mullol and F. Sagués, *Soft Matter*, 2011, **7**, 5109–5112.
115 C. Wilhelm, J. Browaeys, A. Ponton and J.-C. Bacri, *Phys. Rev. E: Stat. Phys., Plasmas, Fluids, Relat. Interdiscip. Top.*, 2003, **67**, 011504.
116 C. Wilhelm, *Phys. Rev. Lett.*, 2008, **101**, 028101.
117 T. Petit, L. Zhang, K. E. Peyer, B. E. Kratochvil and B. J. Nelson, *Nano Lett.*, 2012, **12**, 156–160.
118 P. Tierno, S. Schreiber, W. Zimmermann and T. M. Fischer, *J. Am. Chem. Soc.*, 2009, **131**, 5366–5367.
119 G. Halsz, B. Gyre, I. M. Jnosi, K. G. Szab and T. Tl, *Am. J. Phys.*, 2007, **75**, 1092–1098.
120 A. Terray, J. Oakey and D. W. M. Marr, *Science*, 2002, **296**, 1841.
121 P. Tierno, R. Muruganathan and T. M. Fischer, *Phys. Rev. Lett.*, 2007, **98**, 028301.
122 T. Sawetzki, S. Rahmouni, C. Bechinger and D. W. M. Marr, *Proc. Natl. Acad. Sci. U. S. A.*, 2008, **105**, 20141–20145.
123 B. Kavcic, D. Babic, N. Osterman, B. Podobnik and I. Poberaj, *Appl. Phys. Lett.*, 2009, **95**, 023504.
124 E. M. Purcell, *Am. J. Phys.*, 1977, **45**, 3.
125 O. S. Pak, W. Gao, J. Wang and E. Lauga, *Soft Matter*, 2011, **7**, 8169–8181.
126 P. Fischer and A. Ghosh, *Nanoscale*, 2011, **3**, 557–563.
127 R. Dreyfus, J. Baudry, M. L. Roper, M. Fermigier, H. A. Stone and J. Bibette, *Nature*, 2005, **437**, 862–865.
128 W. Gao, S. Sattayasamitsathit, K. M. Manesh, D. Weihs and J. Wang, *J. Am. Chem. Soc.*, 2010, **132**, 14403–14405.
129 W. Gao, D. Kagan, O. S. Pak, C. Clawson, S. Campuzano, E. C. Erdene, E. Shipton, E. E. Fullerton, L. Zhang, E. Lauga and J. Wang, *Small*, 2012, **8**, 460–467.
130 A. Ghosh and P. Fischer, *Nano Lett.*, 2009, **9**, 2243–2245.
131 D. Schamel, M. Pfeifer, J. G. Gibbs, B. Miksch, A. G. Mark and P. Fischer, *J. Am. Chem. Soc.*, 2013, **135**, 12353–12359.
132 L. Zhang, J. J. Abbott, L. Dong, B. E. Kratochvil, D. Bell and B. J. Nelson, *Appl. Phys. Lett.*, 2009, **94**, 064107.
133 L. Zhang, J. J. Abbott, L. Dong, K. E. Peyer, B. E. Kratochvil, H. Zhang, C. Bergeles and B. J. Nelson, *Nano Lett.*, 2009, **9**, 3663–3667.
134 N. Casic, N. Quintero, R. A. Nodarse, F. G. Mertens, L. Jibuti, W. Zimmermann and T. M. Fischer, *Phys. Rev. Lett.*, 2013, **110**, 168302.
135 P. Tierno, R. Golestanian, I. Pagonabarraga and F. Sagués, *Phys. Rev. Lett.*, 2008, **101**, 218304.
136 P. Tierno, R. Golestanian, I. Pagonabarraga and F. Sagués, *Phys. Rev. E: Stat. Phys., Plasmas, Fluids, Relat. Interdiscip. Top.*, 2010, **81**, 011402.
137 H. Morimoto, T. Ukai, Y. Nagaoka, N. Grobert and T. Maekawa, *Phys. Rev. E: Stat. Phys., Plasmas, Fluids, Relat. Interdiscip. Top.*, 2008, **78**, 021403.
138 C. E. Sing, L. Schmid, M. F. Schneider, T. Franke and A. Alexander-Katz, *Proc. Natl. Acad. Sci. U. S. A.*, 2010, **12**, 535–540.
139 L. Zhang, T. Petit, Y. Lu, B. E. Kratochvil, K. E. Peyer, R. Pei, J. Lou and B. J. Nelson, *ACS Nano*, 2010, **4**, 6228.
140 P. Tierno, R. Golestanian, I. Pagonabarraga and F. Sagués, *J. Phys. Chem. B*, 2008, **112**, 16525–16528.
141 T. R. Kline, W. F. Paxton, T. E. Mallouk and A. Sen, *Angew. Chem., Int. Ed.*, 2005, **44**, 744–746.
142 J. Palacci, S. Sacanna, A. P. Steinberg, D. J. Pine and P. M. Chaikin, *Science*, 2013, **339**, 936–940.
143 R. F. Ismagilov, A. Schwartz, N. Bowden and G. M. Whitesides, *Angew. Chem., Int. Ed.*, 2002, **41**, 652.
144 W. F. Paxton, K. C. Kistler, C. C. Olmeda, A. Sen, S. K. S. Angelo, Y. Cao, T. E. Mallouk, P. E. Lammert and V. H. Crespi, *J. Am. Chem. Soc.*, 2004, **126**, 13424.
145 S. Fournier-Bidoz, A. C. Arsenult, I. Manners and G. A. Ozin, *Chem. Commun.*, 2005, 441.
146 J. R. Howse, R. A. L. Jones, A. J. Ryan, T. Gough, R. Vafabakhsh and R. Golestanian, *Phys. Rev. Lett.*, 2007, **99**, 048102.
147 S. J. Ebbens and J. R. Howse, *Soft Matter*, 2010, **6**, 726–738.
148 L. Baraban, D. Makarov, O. G. Schmidt, G. Cuniberti, P. Leiderer and A. Erbe, *Nanoscale*, 2013, **5**, 1332–1336.
149 G. Zhao, S. Sanchez, O. G. Schmidt and M. Pumera, *Chem. Commun.*, 2012, **48**, 10090–10092.
150 G. Zhao, H. Wang, S. Sanchez, O. G. Schmidt and M. Pumera, *Chem. Commun.*, 2013, **49**, 5147–5149.
151 G. Zhao and M. Pumera, *Langmuir*, 2013, **29**, 7411–7415.
152 V. G. Gradilla, J. Orozco, S. Sattayasamitsathit, F. Soto, F. Kuralay, A. Pourazary, A. Katzenberg, W. Gao, Y. Shen and J. Wang, *ACS Nano*, 2013, **7**, 9232–9240.
153 J. Burdick, R. Laocharoensuk, P. M. Wheat, J. D. Posner and J. Wang, *J. Am. Chem. Soc.*, 2008, **130**, 8164–8165.
154 J. Palacci, S. Sacanna, A. Vatchinsky, P. M. Chaikin and D. J. Pine, *J. Am. Chem. Soc.*, 2013, **135**, 15978.

